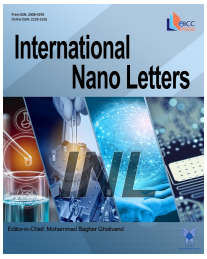

Volume 15, Issue 1, 152503 (1-8)

International Nano Letters (INL)

https://doi.org/10.57647/inl.2025.1401.03

Zinc Oxide Nanoparticles Assembling by a Green Chemistry Method

Adrien Bonneau[1], Marie-Angèle Frémy[1], Sylvie Villain[1], Gilles Baratto[2], Vincent Cot[2], Patricia Merdy[1,*]

[1] *Université de Toulon, Aix Marseille Univ., CNRS, IM2NP, Toulon, France.*
[2] *Véolia Eau, Var Provence Méditerranée, La Garde, France.*

[*] **Corresponding author:** merdy@univ-tln.fr

Original Research

Received:
12 January 2025
Revised:
28 February 2025
Accepted:
17 March 2025
Published in Issue:
31 March 2025

Abstract:

Zinc oxide is a semiconductor material with an interesting potential for photocatalysis of organic pollutants. It has been prepared according an eco-friendly green method, using five various plant extracts (banana, rosemary, bitter orange, olive tree, comfrey). Two different synthesis processes were tested: a hotplate synthesis and a hydrothermal method. Metal precursor used was zinc acetate. Plants present in the process allowed the formation and the self-assembling of ZnO during the crystal growth thanks to the large chemical family of polyphenol which act as reductants. Crystalline and organic matter-free compounds obtained after annealing were characterized with diffractive reflectance spectroscopy (DRS) to determine gap energies and confirm ZnO belonging to semiconductors, X-ray diffraction to verify the crystalline structure and its features, Fourier transform infrared spectroscopy (FTIR) to check the characteristic functional group and scanning electron microscopy (SEM) to reveal the self-assembling forms of ZnO. Data about the shapes, dimensions and crystal planes of zinc oxide were regarded in the light of the plant and the synthesis method used. This work has highlighted the morphologies of ZnO obtained on the basis of the synthesis method and the plant extracts.

Keywords: Zinc oxide; Green-chemistry; Synthesis method; Plant extracts

Cite this article: Bonneau, A., Frémy, M.-A., Villain, S., Baratto, G., Cot, V., Merdy, P. Zinc Oxide Nanoparticles Assembling by a Green Chemistry Method. *Int. Nano Lett.* **15**(1), 152503 (2025).

1. Introduction

Zinc oxides are semiconductor materials possessing a wide band gap energy (3.37 eV) which confers a high capacity of UV light absorption [1]. Thanks to its optic and electronic properties, it is used in a variety of applications: solar cells [2], gas sensors [3], photodiodes [4], piezoelectricity [5, 6], agriculture [7], antibacterial activity [8], medicine [9, 10] or photocatalysis [11].

Chemical methods used to synthesize zinc oxide are various: hydrothermal [12], sol-gel [13], co-precipitation [14], green fabrication route [15], sonochemical [16] to name a few. Furthermore, these methods allow to get a profusion of ZnO assemblies like spheres, flowers, wires or cages [17], granting a promising path for photocatalysis applications.

The use of green material implies plants [18], fungi [19], algae [20] or bacteria [21]. Apart from having green waste, it is beneficial because this material contains organic molecules capable of chelating metals and forming oxide nanoparticles with morphology variations [22]. Using plants, the involved molecules are antioxidants such as polyphenols, flavonoids, vitamins, alkaloids, amino and carboxylic acid groups are found in the whole vegetal world, where the first ones act like reducing and chelating agents, the others like stabilizers [23]. This is notably the case for the plants used in the current study belonging to different botanic families with specific chelating agents such as flavonoids or tannic acids (Table 1): *Citrus aurantium* (bitter orange) and *Musa acuminata* (banana) fruit peels, *Salvia rosmarinus* (rosemary), *Olea europaea* (olive tree) and *Symphytum officinale* (comfrey) leaves. Therefore, besides the chelating molecule, chemical mechanims involved in zinc complexes formation mainly depend on the stability constants of the polyphenols under pH [24], where the zinc complexe geometry is generally tetrahedral or octahedral [25] according to the ligand availability and steric hindrance

constraints.
Beyond this work, the aim is to reach morphological assembly of zinc oxide suitable for heterogeneous photocatalysis. Indeed, SEM studies will help furthermore to define the more appropriate forms including synthesis parameters like plant species and their chemical composition and chemical method, although other factors like temperature, reaction time, pH of the synthesis, precursor and plant concentration, drying parameters and calcination programing are also important aspects to study to form ZnO.

2. Materials and methods

2.1 Preparation of plant extracts

Mediterranean climate suited plants were gathered from the natural environment. The banana constitutes an exception in this study and was provided from a greengrocer. The preliminary step consisted of washing the plants with deionized (DI) water then drying plant parts separately (fruit, leaves, flowers, stems) with a low-temperature oven at 60 °C. Some plants needed an additional preparation before drying. For fruit like bitter orange or banana, the plant extract was composed of the outer peel. The bright-colored epicarp was insulated by using a knife. Then, plant parts were thinly grinded in the case of leaves or sliced for peels.
The synthesis of the plant extract occured as follows: 3 g of dried plant were added to 50 mL of DI water, then the mixture was heated at 70 °C for 15 minutes. A clear change in aqueous solution color indicated that the active substances has been extracted (Fig. 1), those are different among plant extracts due to the diversity of molecules present in the vegetal world. The extract was filtered (Whatman paper, pore size 25 µm, diameter 55 mm) and stored at 4 °C. The scheme of the synthesis is showed in the Fig. **??**.

2.2 Zinc oxide synthesis

50 mL of deionized water was added to 0.2 M dihydrated zinc acetate ($[Zn(OOCCH_3)_2{\cdot}2H_2O]$, Carlo Erba). The aqueous solution was laid onto a magnetic hotplate stirrer. Only the stirring function was activated for the first 10 minutes. Next, 10 mL of the plant extract was brought to the solution (Fig. 2). The color of the mixture was different according to the plant or the zinc precursor. Then, the heating function was on at 70 °C for 2 hours keeping the magnetic stirring. A part of the solution volume was evaporated by heating. The metal complexation with oxidizing molecules from plants may be visible with a progressive change of color in the solution. Finally, the mixture was placed into a low temperature oven at 60 °C leaving the water evaporated. Shiny grey zinc compounds appeared during this step with a visible presence of organic matter characterized by brown spots (Fig. **??**). In order to remove organic matter, the dry residue was calcinated at 400 °C for 2 hours in an oven (Nabertherm-Model P330). Peculiarly, this step allowed to free zinc oxides, in accordance with future DRX results which were separated from residual water and chelating agents. The dry oxide powder obtained was finally stored at room temperature in a 5 mL pillbox in the dark for any further characterization and photocalysis use. For each sample synthesized using an open-air system through the hotplate route, their equivalent was made by the hydrothermal method or closed-air system. For this, 32 mL of DI water was added to 1.6 g zinc acetate as well as 8 mL plant extract. The mixing was placed into a PTFE liner and a bombshell. The heating function was activated at 120 °C for 18 hours and under continuous stirring at 800 rpm. The next steps followed the basic drying and calcination protocol mentioned above.

2.3 Zinc oxide characterization

The energy gap of semiconductors ZnO were found with Diffuse Reflectance Spectroscopy (DRS) using the UV-2600i SHIMADZU device coupled to the integrated sphere. The employed wavelength range were from 200 to 700 nm in the case of ZnO materials.
The chemical structure of oxide powders have been determined by X-ray Diffraction using a Philips X'Pert diffractometer. The copper anti-cathode ($\lambda = 1.5406$ Å) is bombarded with a 40 kV X-ray electron generator. The measurements have been conducted with a 2θ angular range of $15 - 75°$. XRD data have been processed on the software HighScore. We obtained additional data from these analyses: Cell parameters and crystal particle sizes.
Pictures of nanoparticles were obtained using Scanning Electron Microscopy (SEM) with a 5 kV In-lens detector. The device was a Zeiss-Supra 40 VP/Gemini column functioning with an incident electron beam. It allowed to overview the assemblage of ZnO particles, where parameters like the morphology and particle size are points to consider. Metallization was not employed into sample treatment and explain the possible charge effect seen in SEM pictures due to an accumulation of electrons on the surface of the powder.
FTIR spectroscopy allows to check the functional groups and vibrational modes of ZnO. The FTIR spectra were recorded with the model Alpha II from Bruker in the $4000 - 400$ nm wavelength range.

3. Results and discussion

The sample names are summarized in the Table 2.

3.1 XRD study

The XRD diagrams of the plant-based ZnO are showed in Fig. 3. They all exhibited a regular set of peaks, confirming the hexagonal closed-packed structure of ZnO corresponding to the wurtzite-type structure with the space group of $P6_3mc$ according to the Hermann-Mauguin notation and its international number No. 186. The reference data in the JCPDS card (No. 36-1451) was related to the reference ZnO. Therefore, the corresponding peaks associated with the Miller indices were (100) for 31.8°, (002) for 34.4°, (101) for 36.3°, (102) for 47.6°, (110) for 56.6°, (103) for 62.9°, (200) for 66.4°, (112) for 68° and (201) for 69.1°. Concerning ZnO formed with banana and comfrey, another mineral appeared in very low quantities. It can be attributed to the sylvite KCl with main peaks at 28.3° and 40.5°. The formation of this mineral probably occurs during calcination at 400 °C while the rest of organic matter is annealed. The Debye-Scherrer formula was used to calculate the av-

erage particle size thanks to the mean size $D = k\lambda/\beta\cos\theta$, with k the shape factor, λ the wavelength (nm), β the full width at half maximum (FWHM) and θ the Bragg angle (°). The results are given in Table 3. The cell volume V was calculated with the parameter a the side length of the hexagonal basis and the parameter c the height of the unit cell:

$$V = \frac{\sqrt{3}}{2} \times a^2 \times c \quad (1)$$

According to the figures 3 and 5, the XRD peak intensities show a preferential lattice orientation for the (101) plane for all samples. In fact, there are few differences between experiments whether for the chemical method or the plant parameter. The Table 4 expresses well the similarities of data with statistic results thanks to a ratio calculation with the (002) plane, the lowest intensity value. Refering to the figure 4, the lattice plane (002) is parallel to the plane containing the Zn and O atoms, whereas the lattice plane (100) is perpendicular to the (002) plane. The preferential lattice orientation according to the (002) plane is usually obtained by physico-chemical methods like pulsed laser deposition [26] with formation of ZnO thin films or ultrasonic spray pyrolysis [27] thanks to the crystal growth specifically oriented on substrates.

3.2 Gap energy E_g

Diffusive Reflectance Spectroscopy (DRS) was used to determine the energy band gap of ZnO. According to the figure8 6 (a), it was observed that ZnO did not absorb a lot in visible light with a cut-off wavelength shift from 420 nm to 370 nm. The Tauc plot's formula allowed to find the gap energy E_g [28]:

$$\alpha h\nu = A(h\nu - E_g)^n \quad (2)$$

α is the absorption coefficient, h the Planck constant, ν the photon energy and A is a constant. ZnO generally exhibits a direct band gap which means $n = 1/2$, as it is for hexagonal wurtzite structure. In cases of high pressure crystal formation like the cubic rocksalt structure, zinc oxide owns and indirect band gap [29, 30]. The values of energy band gaps for ZnO varied between 3.28 and 3.30 eV (Table 5). These results are relevant with the range of ZnO band gap found in publications [31, 32].

3.3 FTIR

The FTIR spectra of two ZnO samples are shown in the Fig. 7. Banana peels were employed in the syntheses of these samples. Both spectra appeared quite similar: The peaks at 3420 cm^{-1} and 2912 cm^{-1} are related to hydroxyl groups, including H_2O [33] on the nanoparticle surface. Similarly, as the previous are -OH stretching, the peaks at 1058 and 852 cm^{-1} fit -OH bendings [34, 35]. The band at 2342 cm^{-1} is correlated to the stretching mode of gaseous CO_2 [36]. The vibrations with organic functional groups are due to the residual plant extract or from the precursor after calcination and correspond at 1375 cm^{-1} to ester group O-C-O stretching vibrations, and at 1578 cm^{-1} to carboxyl group O-C=O [36], whereas the peak at 1491 cm^{-1} refers to C-H bending [37].

The great slope fall occuring between 450 and 400 cm^{-1} is attributed to the bond Zn-O [38].

3.4 Synthesis method and plant impacts

Different ZnO morphologies were obtained according to hotplate versus hydrothermal use and evenly according to different plant extracts. They are represented in figure8 (SEM pictures). ZnO phases and energy gaps data (Table 4) were the same regardless of the method used (hotplate vs. hydrothermal). Actually the main difference consisted in the microscopic assembly of ZnO particles which offered differentiated morphologies. ZnO@Ban (Fig. 8 (E-F)) and ZnO@Oli (Fig. 8 (G-H)) were composed of large pencil forms with little difference between the hotplate and the hydrothermal method. ZnO@Com (Fig. 8 (I-J)) showed more elongated pencils in the hotplate synthesis and in addition a strong presence of long nanorods in the hydrothermal one. The samples with rosemary (Fig. 8 (C-D)) revealed for hydrothermal method some nanorod arrangements of the same stripe as ZnO@hyd-Com, and for heating plate some egg-like morphology. ZnO@Ora (Fig. 8 (A-B) presents a broader choice of nanoparticle forms in both heating plate and hydrothermal syntheses with pencils, nanorods and especially egg-like particles. In reference to the Table 1, plants consist mainly of polyphenols and could explain that the shaped obtained are not so different between samples.
The comparison between dimensions of SEM particles and crystalite sizes according to the (100) and (002) lattice plans determined with the XRD was shown (Table 5) and exhibited good similarities. In Figure 10, for instance ZnO@hyd-Ban (F) and ZnO@heat-Com (I) showed respectively pencils with large base and elongated c-axis. They have the highest values in crystalite size calculated in Table 3 (68.86 and 73.12 nm). Compared with ZnO@hyd-Ora (B), forms of flower petals seemed to be very large but the presence of additional smaller different particles in the sample explain a restricted XRD value (58.19 nm).
For each sample, the crystallite size according to the lattice planes (100) and (002) (see Fig. 4) was reckoned in Table 6 according to the full width at half maximum (FWHM) calculation. The symbol L represents the length of the hexagonal closed-packed structure of the ZnO whereas the symbol D is for the diameter of the particle. The calculated ratio L/D directly reports on the form of the crystallite according to the plant and the synthesis method. The lattice plane (100) showed remarkably constant sizes except for the bitter orange ones with larger diameters. Then, it has been deducted that most of the samples have stretched particles with L/D ratio between 2 and 3. However, the most packed ZnO were correlated with bitter orange-made ZnO and a L/D ratio closer to 1, with a great presence of more pseudo-spherical particles, which was also the best photocatalytic material. The influence of the chemical method was less significant than the plant used. Regarding the SEM size measurements, The image processing and analysis software Fiji was used in order to estimate the range of the particle size found in each sample, with about a hundred measures of medium-size particles and a 20.000x magnification. It is interesting to notice that the measured axis 'a' was well correlated

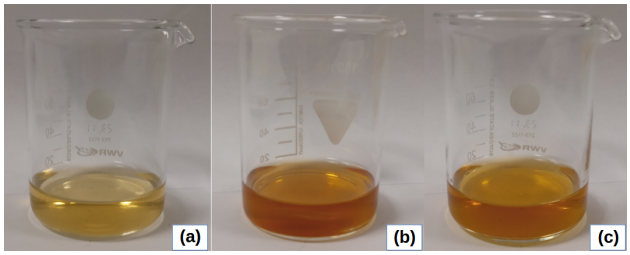

Figure 1. Examples of used plant extracts after 15 minutes heating (70 °C) (a) Rosemary, (b) Banana, (c) Olive tree.

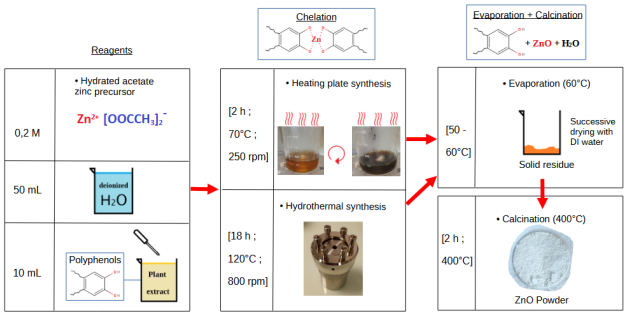

Figure 2. Green synthesis of zinc oxide nanoparticles.

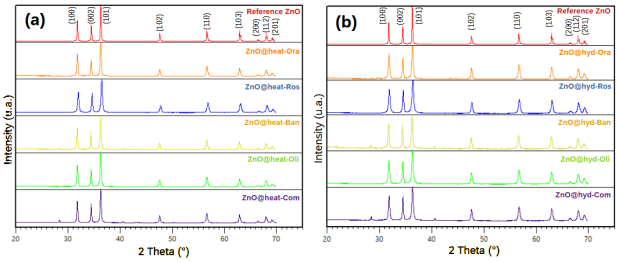

Figure 3. XRD patterns of standard ZnO and synthesized ZnO: (a) hotplate syntheses of ZnO ; (b) hydrothermal syntheses of ZnO.

with XRD calculated crystallite size, with the bottom of the range approximately equal to the lattice plane (100). This was less obvious for the measured range axis 'c' because of the stack growth of particles especially along this axis, hindering borders of the crystallites and making harder the estimation.

4. Conclusion

Zinc oxide has been successfully synthesized by a green process using a plant extract as confirmed by the cristalline structure determined by X-ray diffraction. On the other hand, this work has highlighted the morphologies of ZnO obtained on the basis of the synthesis method and the plant extract. If the cristalline structure and gap energies are substancially the same, nanoparticle SEM measurements showed some contrasts in shapes and size, essentially with the bitter orange-made samples where XRD major peak intensities are also different from the other ones. As a conclusion, discrepancies are especially visible for the plant parameter but very little concerning the chemical method. A possible continuation of this work would be to experiment the photocatalytic activities of these oxides under UV-visible light in order to correlate their

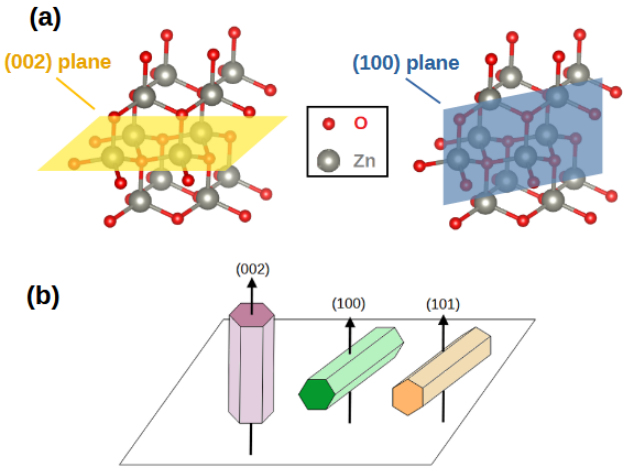

Figure 4. (a) Lattice placement of (002) and (100) on the hexagonal closed-packed wurtzite structure of ZnO (modified from [47]) (b) Main lattice planes orientation adopted by the phase wurtzite of ZnO (modified from [48]).

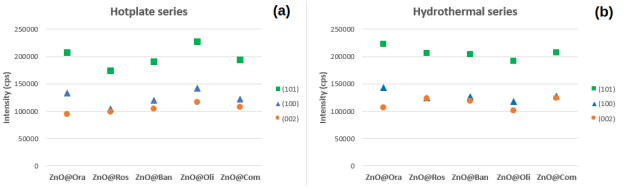

Figure 5. Relative XRD intensities of (100), (002) and (101) lattice planes for ZnO according to hotplate (a) and hydrothermal (b) syntheses.

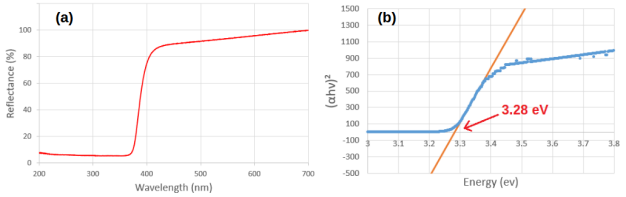

Figure 6. (a) Diffusive reflectance spectrum and (b) Tauc plot of ZnO@hyd-Ros.

performance.

Funding

This work was financially supported by Véolia through a PhD grant and by Agence de l'Eau Rhône Méditerranée Corse (AERMC).

Ethical approval

The project had approved by the research ethics committee of Semnan University of Medical Sciences (approval ID: IR.SEMUMS.REC.1401.222).

Authors Contribution

Authors have contributed equally in preparing and writing the manuscript.

Availability of data and materials

The data that support the findings of this study are available from the corresponding author, upon reasonable request.

Table 1. Phytochemical composition of plant extracts.

Name	Latin Name	Family	Part used	Main chemical constituents	References
Rosemary	Salvia rosmarinus	Lamiaceae	Leaves	Flavonoids, essential oils, phenolic acids, terpenes, polysaccharides	[39, 40]
Banana	Musa acuminata	Musaceae	Peel	Phenolic acids, carotenoids, aminoacids	[41]
Bitter orange	Citrus aurantium	Rutaceae	Peel	Flavonoids, alkaloids, essential oils, coumarins	[42, 43]
Olive tree	Olea europa	Oleaceae	Leaves	Flavonoids, phenolic componds, terpenes	[44]
Comfrey	Symphytum officinale	Boraginaceae	Leaves	Mucilage, tannins, alkaloids, phenolic acids, polysaccharides, terpenes, steroids	[45, 46]

Table 2. Terminology to describe the sample names.

	Plant	**Latin name**
ZnO@Ros	Rosemary	*Salvia rosmarinus*
ZnO@Ban	Banana	*Musa acuminata*
ZnO@Ora	Bitter Orange	*Citrus aurantium*
ZnO@Oli	Olive tree	*Olea europaea*
ZnO@Com	Comfrey	*Symphytum officinale*

	Mean
ZnO@heat-	Synthesis by heating plate method
ZnO@hyd-	Synthesis by hydrothermal method

Table 3. Cristallite size (unit: Å) using the Debye-Scherrer formula.

Sample	Parameter a (nm)	Parameter c (nm)	V (nm^3)	Crystallite size (nm)
ZnO@heat-Ora	0.3250	0.5208	0.0476	54.46
ZnO@hyd-Ora	0.3248	0.5203	0.0475	58.19
ZnO@heat-Ros	0.3241	0.5193	0.0472	62.6
ZnO@hyd-Ros	0.3246	0.5200	0.0474	57.53
ZnO@heat-Ban	0.3251	0.5208	0.0477	61.25
ZnO@hyd-Ban	0.3252	0.5210	0.0477	68.86
ZnO@heat-Oli	0.3250	0.5207	0.0476	59.72
ZnO@hyd-Oli	0.3248	0.5204	0.0475	54.26
ZnO@heat-Com	0.3251	0.5229	0.0479	73.12
ZnO@hyd-Com	0.3240	0.5207	0.0473	63.14

Mean crystallite size (nm)	**Confidence interval 95%**	
61.31	Lower bound (nm)	Upper bound (nm)
	57.83	64.79

Conflict of interests
The authors declare that they have no known competing financial interests or personal relationships that could have appeared to influence the work reported in this paper.

Table 4. XRD peak intensities ratio of (100), (002) and (101) lattice planes.

	Hotplate system series			Hydrothermal system series	
	$I_{(101)} / I_{(002)}$	$I_{(100)} / I_{(002)}$		$I_{(101)} / I_{(002)}$	$I_{(100)} / I_{(002)}$
ZnO@heat-Ora	2.21	1.42	ZnO@hyd-Ora	2.08	1.34
ZnO@heat-Ros	1.76	1.05	ZnO@hyd-Ros	1.67	1.00
ZnO@heat-Ban	1.82	1.14	ZnO@hyd-Ban	1.72	1.07
ZnO@heat-Oli	1.95	1.22	ZnO@hyd-Oli	1.90	1.17
ZnO@heat-Com	1.79	1.13	ZnO@hyd-Com	1.67	1.03
Mean	1.905	1.192	Mean	1.809	1.123
Standard deviation	0.164	0.126	Standard deviation	0.161	0.123
Lower bound (C.I. 95%)	1.730	1.058	Lower bound (C.I. 95%)	1.638	0.991
Upper bound (C.I. 95%)	2.080	1.327	Upper bound (C.I. 95%)	1.980	1.254

Table 5. Gap energies of the ZnO samples with: (a) ZnO by the hotplate method; (b) ZnO by the hydrothermal method ; (c) the statistic values were obtained for calculated energy gaps with three decimals (here E_g displayed with two decimals).

(a)

	Eg
ZnO@heat-Ros	3.28
ZnO@heat-Ban	3.29
ZnO@heat-Ora	3.28
ZnO@heat-Oli	3.29
ZnO@heat-Com	3.29

(b)

	Eg
ZnO@hyd-Ros	3.30
ZnO@hyd-Ban	3.30
ZnO@hyd-Ora	3.28
ZnO@hyd-Oli	3.29
ZnO@hyd-Com	3.30

(c)

Mean	Confidence interval 95%	
	Lower bound	Upper bound
3.2903	3.2864	3.2951

Table 6. Crystallite and assembly size of the particle samples from SEM and XRD measurements.

	XRD crystallite dimensions			SEM assembly size	
Sample	(100) lattice plane (nm)	(002) lattice plane (nm)	L/D	Measured range of a-axis stacks (nm)	Measured range of c-axis stacks (nm)
ZnO@heat-Ora	43.7	61.2	1.40	40-90	100-200
ZnO@hyd-Ora	63.5	67.1	1.06	50-140	100-300
ZnO@heat-Ros	33.3	59.4	1.78	30-55	60-180
ZnO@hyd-Ros	34.3	83.2	2.43	30-50	100-200
ZnO@heat-Ban	35.3	94.5	2.68	30-50	150-600
ZnO@hyd-Ban	36.3	94.5	2.60	20-45	150-400
ZnO@heat-Oli	37.3	74.3	1.99	40-70	150-500
ZnO@hyd-Oli	38.3	83.2	2.17	20-35	80-300
ZnO@heat-Com	39.3	94.5	2.40	20-45	200-500
ZnO@hyd-Com	40.3	109.5	2.72	30-45	100-250

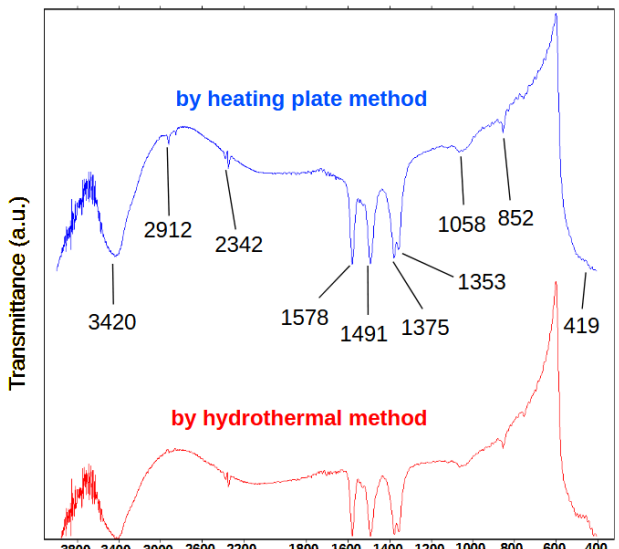

References

[1] V. Vaiano, M. Matarangolo, J.J. Murcia, H. Rojas, J.A. Navío, and M.C. Hidalgo. Enhanced photocatalytic removal of phenol from aqueous solutions using ZnO modified with Ag. . *Applied Catalysis B: Environmental*, **225**:197–206, (2018). DOI: https://doi.org/10.1016/j.apcatb.2017.11.075.

[2] C. Lin, H. Lin, J. Li, and X. Li. Electrodeposition preparation of ZnO nanobelt array films and application to dye-sensitized solar cells. *Journal of Alloys and Compounds*, **462**:175–180, (2008). DOI: https://doi.org/10.1016/j.jallcom.2007.07.104.

[3] P.S. Cho, K.W. Kim, and J.H. Lee. NO_2 sensing characteristics of ZnO nanorods prepared by hydrothermal method. *J Electroceram*,

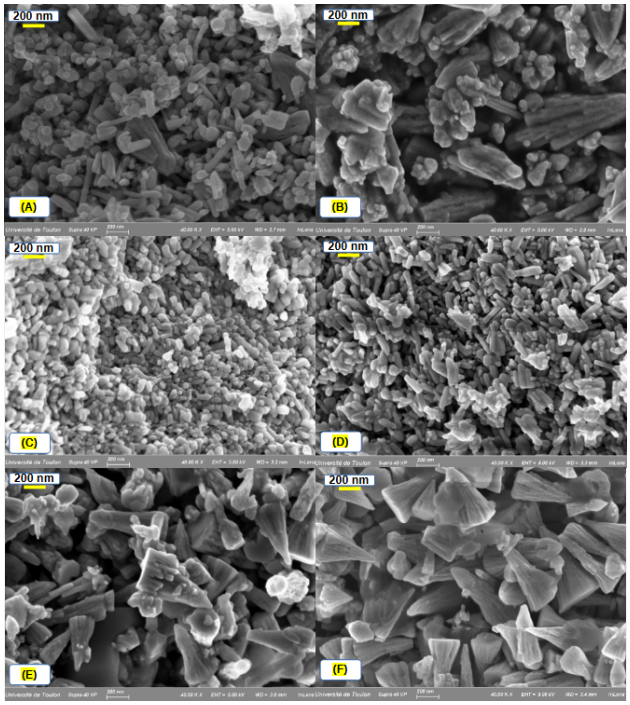

Figure 8. SEM images of ZnO samples according to different plant extracts and hotplate vs hydrothermal synthesis; (A) ZnO@heat-Ora; (B) ZnO@hyd-Ora; (C) ZnO@heat-Ros; (D) ZnO@hyd-Ros; (E) ZnO@heat-Ban; (F) ZnO@hyd-Ban; (G) ZnO@heat-Oli; (H) ZnO@hyd-Oli; (I) ZnO@heat-Com; (J) ZnO@hyd-Com.

17:975–978, (2006).
DOI: https://doi.org/10.1007/s10832-006-8146-7.

[4] L. Luo, Y. Zhang, S.S. Mao, and L. Lin. Fabrication and characterization of ZnO nanowires based UV photodiodes. . *Sensors and Actuators A: Physical*, **127**:201–206, (2006).
DOI: https://doi.org/10.1016/j.sna.2005.06.023.

[5] R.K. Pandey, J. Dutta, S. Brahma, B. Rao, and C.P. Liu. Review on ZnO-based piezotronics and piezoelectric nanogenerators: Aspects of piezopotential and screening effect. . *Journal of Physics: Materials*, **4**:044011, (2021).
DOI: https://doi.org/10.1088/2515-7639/ac130a.

[6] L.Z. Kou, W.L. Guo, and C. Li. Piezoelectricity of ZnO and its nanostructures. . *Symposium on Piezoelectricity, Acoustic Waves, and Device Applications, Nanjing, China*, pages 354–359, (2008).
DOI: https://doi.org/10.1109/SPAWDA.2008.4775808.

[7] T.N.V.K.V. Prasad, P. Sudhakar, Y. Sreenivasulu, P. Latha, V. Munaswamy, K.R. Reddy, T.S. Sreeprasad, P.R. Sajanlal, and T. Pradeep. Effect of nanoscale zinc oxide particles on the germination, growth and yield of peanut. *Journal of Plant Nutrition*, **35**:905–927, (2012).
DOI: https://doi.org/10.1080/01904167.2012.663443.

[8] Y.H. Leung, X. Xu, A.P.Y. Ma, F. Liu, A.M.C. Ng, Z. Shen, L.A. Gethings, M.Y. Guo, A.B. Djurisic, P.K.H. Lee, H.K. Lee, W.K. Chan, and F.C.C. Leung. Toxicity of ZnO and TiO_2 to Escherichia coli cells. . *Sci*, **6**:35243, (2016).
DOI: https://doi.org/10.1038/srep35243.

[9] A. Nazarizadeh and S. Asri-Rezaie. Comparative Study of Antidiabetic Activity and Oxidative Stress Induced by Zinc Oxide Nanoparticles and Zinc Sulfate in Diabetic Rats. . *AAPS Pharm Sci Tech*, **17**:834–843, (2016).
DOI: https://doi.org/10.1208/s12249-015-0405-y.

[10] S. Mitra, B. Subia, P. Patra, S. Chandra, N. Debnath, S. Das, R. Banerjee, S.C. Kundu, P. Pramanik, and A. Goswami. Porous ZnO nanorod for targeted delivery of doxorubicin: *in vitro* and *in vivo* response for therapeutic applications. *J. Mater. Chem.*, **22**:24145–24154, (2012).
DOI: https://doi.org/10.1039/C2JM35013K.

[11] M. Imran Din, R. Khalid, J. Najeeb, and Z. Hussain. Fundamentals and photocatalysis of methylene blue dye using various nanocatalytic assemblies- a critical review. . *Journal of Cleaner Production*, **298**:126567, (2021).
DOI: https://doi.org/10.1016/j.jclepro.2021.126567.

[12] A. Ejsmont and J. Goscianska. Hydrothermal Synthesis of ZnO Superstructures with Controlled Morphology via Temperature and pH Optimization. *Materials (Basel)*, **16**:1641, (2023).
DOI: https://doi.org/10.3390/ma16041641.

[13] J.N. Hasnidawani, H.N. Azlina, H. Norita, N.N. Bonnia, S. Ratim, and E.S. Ali. Synthesis of ZnO Nanostructures Using Sol-Gel Method. . *Procedia Chemistry*, **19**:211–216, (2016).
DOI: https://doi.org/10.1016/j.proche.2016.03.095.

[14] R.E. Adam, G. Pozina, M. Willander, and O. Nur. Synthesis of ZnO nanoparticles by co-precipitation method for solar driven photodegradation of Congo red dye at different pH. *Photonics and Nanostructures-Fundamentals and Applications*, **32**:11–18, (2018).
DOI: https://doi.org/10.1016/j.photonics.2018.08.005.

[15] L. Fu and Z. Fu. Plectranthus amboinicus leaf extract–assisted biosynthesis of ZnO nanoparticles and their photocatalytic activity. *Ceramics International*, **41**:2492–2496, (2015).
DOI: https://doi.org/10.1016/j.ceramint.2014.10.069.

[16] K. Zak, W.H.A. Majid, H.Z. Wang, R. Yousefi, A.M. Golsheikh, and Z.F. Ren. Sonochemical synthesis of hierarchical ZnO nanostructures.". *Ultrasonics Sonochemistry*, **20**:395–400, (2013).
DOI: https://doi.org/10.1016/j.ultsonch.2012.07.001.

[17] H. Gulab, N. Fatima, U. Tariq, O. Gohar, M. Irshad, M.Z. Khan, M. Saleem, A. Ghaffar, M. Hussain, A.K. Jan, M. Humayun, M. Motola, and M.B. Hanif. Advancements in zinc oxide nanomaterials: Synthesis, properties, and diverse applications. *Nano-Structures & Nano-Objects*, **39**:101271, (2024).
DOI: https://doi.org/10.1016/j.nanoso.2024.101271.

[18] B. Naiel, M. Fawzy, A.E.D. Mahmoud, and M.W.A. Halmy. Sustainable fabrication of dimorphic plant derived ZnO nanoparticles and exploration of their biomedical and environmental potentialities. . *Sci Rep.*, **14**:13459, (2024).
DOI: https://doi.org/10.1038/s41598-024-63459-0.

[19] M.P.N. Rao. Chapter 5 - Fungal synthesis of zinc oxide nanoparticles and its applications in biomedical, environmental, and agri-food sectors, Editor(s): Kamel, A. Abd-Elsalam, In Nanobiotechnology for Plant Protection, Fungal Cell Factories for Sustainable Nanomaterials Productions and Agricultural Applications. Elsevier:115–130, (2023).
DOI: https://doi.org/10.1016/B978-0-323-99922-9.00008-8.

[20] H. Hameed, A. Waheed, M.S. Sharif, M. Saleem, A. Afreen, M. Tariq, A. Kamal, W.A. Al-onazi, D.A. Al Farraj, S. Ahmad, and R.M. Mahmoud. Green Synthesis of Zinc Oxide (ZnO) Nanoparticles from Green Algae and Their Assessment in Various Biological Applications. *Micromachines*, **14**:928, (2023).
DOI: https://doi.org/10.3390/mi14050928.

[21] R. Ishwarya, R. Rajaganesh, M. Geetha, G. Kalaiarasi, N. Arul, J. Tharani, K. Kavithaa, and D. Sangeetha. Microbial synthesis of zinc oxide nanoparticles and their potential biological application as an antimicrobial and anticancer agent. . *Biocatalysis and Agricultural Biotechnology*, **62**:103417, (2024).
DOI: https://doi.org/10.1016/j.bcab.2024.103417.

[22] S. Dey, D.L. Mohanty, N. Divya, V. Bakshi, A. Mohanty, D. Rath, S. Das, A. Mondal, S. Roy, and R. Sabui. A critical review on zinc oxide nanoparticles: Synthesis, properties and biomedical applications. *Intelligent Pharmacy*, (2024).
DOI: https://doi.org/10.1016/j.ipha.2024.08.004.

[23] O.J. Nava, C.A. Soto-Robles, C.M. Gómez-Gutiérrez, A.R. Vilchis-Nestor, A. Castro-Beltrán, A. Olivas, and P.A. Luque. Fruit peel extract mediated green synthesis of zinc oxide nanoparticles. *Journal of Molecular Structure*, **1147**:1–6, (2017).
DOI: https://doi.org/10.1016/j.molstruc.2017.06.078.

[24] N.R. Perron and J.L. Brumaghim. A Review of the Antioxidant Mechanisms of Polyphenol Compounds Related to Iron Binding. *Cell Biochem Biophys*, **53**:75–100, (2009).
DOI: https://doi.org/10.1007/s12013-009-9043-x.

[25] A. Krezel and W. Maret. The biological inorganic chemistry of zinc ions. . *Archives of Biochemistry and Biophysics*, **611**:3–19, (2016).
DOI: https://doi.org/10.1016/j.abb.2016.04.010.

[26] J.L. Zhao, X.M. Li, S. Zhang, C. Yang, X.D. Gao, and W.D. Yu. Highly (002)-oriented ZnO film grown by ultrasonic spray pyrolysis on ZnO-seeded Si (100) substrate. . *J. Mater. Res.*, **21**:2185–2190, (2006).
DOI: https://doi.org/10.1557/jmr.2006.0291.

[27] L. Roza, V. Fauzia, and M.Y.A. Rahman. Tailoring the active surface sites of ZnO nanorods on the glass substrate for photocatalytic activity enhancement. *Surfaces and Interfaces*, **15**:117–124, (2019).
DOI: https://doi.org/10.1016/j.surfin.2019.02.009.

[28] S. Abdullahi, S. Güner, Y. Koseoglu, I. Musa, B. Adamu, and M. Abdulhamid. Simple Method For The Determinatıon of Band Gap of a Nanopowdered Sample Using Kubelka Munk Theory. . *Journal of the Nigerian Association of Mathematical Physics*, **35**:241–246, (2016).

[29] D.K. Sharma, S. Shukla, K.K. Sharma, and V. Kumar. A review on ZnO: Fundamental properties and applications. . *Materials Today: Proceedings*, **49**:3028–3035, (2022).
DOI: https://doi.org/10.1016/j.matpr.2020.10.238.

[30] F.S. Saoud, J.C. Plenet, and M. Henini. Band gap and partial density of states for ZnO: Under high pressure. *Journal of Alloys and Compounds*, **619**:812–819, (2015).
DOI: https://doi.org/10.1016/j.jallcom.2014.08.069.

[31] E. Bacaksiz, M. Parlak, M. Tomakin, A. Özcelik, M. Karakız, and M. Altunbas. The effects of zinc nitrate, zinc acetate and zinc chloride precursors on investigation of structural and optical properties of ZnO thin films. . *Journal of Alloys and Compounds*, **466**:447–450, (2008).
DOI: https://doi.org/10.1016/j.jallcom.2007.11.061.

[32] M.A. Gatou, N. Lagopati, I.A. Vagena, M. Gazouli, and E.A. Pavlatou. ZnO Nanoparticles from Different Precursors and Their Photocatalytic Potential for Biomedical Use. . *Nanomaterials (Basel)*, **13**:122, (2022).
DOI: https://doi.org/10.3390/nano13010122.

[33] J. Naradala. Germination and Growth Characteristics of Mungbean Seeds (*Vigna radiata* L.) affected by Synthesized Zinc Oxide Nanoparticles. *International Journal of Current Engineering and Technology*, **4**:3411–3416, (2014).

[34] A. Ashar, I.A. Bhatti, T. Siddique, S.M. Ibrahim, S. Mirza, Z.A. Bhutta, M. Shoaib, M. Ali, M.B. Taj, M. Iqbal, S. Noor, and M. Mohsin. Integrated hydrothermal assisted green synthesis of ZnO nano discs and their water purification efficiency together with antimicrobial activity. . *Journal of Materials Research and Technology*, **15**:6901–6917, (2021).
DOI: https://doi.org/10.1016/j.jmrt.2021.11.009.

[35] D. Thongam, J. Gupta, and N. Sahu. Effect of induced defects on the properties of ZnO nanocrystals: surfactant role and spectroscopic analysis. . *SN Applied Sciences*, **1**:1030, (2019).
DOI: https://doi.org/10.1007/s42452-019-1058-3.

[36] A. Bhapkar, R. Prasad, D. Jaspal, M. Shirolkar, K. Gheisari, and S. Bhame. Visible light driven photocatalytic degradation of methylene blue by ZnO nanostructures synthesized by glycine nitrate auto combustion route. . *Inorganic Chemistry Communications*, **148**:110311, (2023).
DOI: https://doi.org/10.1016/j.inoche.2022.110311.

[37] M.C. Patterson, M.F. Di Tusa, C.A. McFerrin, R.L. Kurtz, R.W. Hall, E.D. Poliakoff, and P.T. Sprunger. Formation of environmentally persistent free radicals (EPFRs) on ZnO at room temperature: Implications for the fundamental model of EPFR generation. *Chemical Physics Letters*, **670**:5–10, (2017).
DOI: https://doi.org/10.1016/j.cplett.2016.12.061.

[38] K. Tanji, J.A. Navio, A. Chaqroune, J. Naja, F. Puga, M.C. Hidalgo, and A. Kherbeche. Fast photodegradation of rhodamine B and caffeine using ZnO-hydroxyapatite composites under UV-light illumination. . *Catalysis Today*, **388-389**:176–186, (2022).
DOI: https://doi.org/10.1016/j.cattod.2020.07.044.

[39] Y. Sharma, R. Velamuri, J. Fagan, and J. Schaefer. Full-Spectrum Analysis of Bioactive Compounds in Rosemary (*Rosmarinus officinalis* L.) as Influenced by Different Extraction Methods. *Molecules*, **25**:4599, (2020).
DOI: https://doi.org/10.3390/molecules25204599.

[40] M.T. Joshua. Phytochemical Constituents of Rosmarinus officinalis Linn. and Their Associated Role in the Management of Alzheimer's Disease. In: Izah, S.C., Ogwu, M.C., Akram, M. (eds) Herbal Medicine Phytochemistry. Reference Series in Phytochemistry. Springer, Cham., (2024).
DOI: https://doi.org/10.1007/978-3-031-21973-3_14-1.

[41] W.M. Hikal, H.A.H. Said-Al Ahl, A. Bratovcic, K.G. Tkachenko, J. Sharifi-Rad, M. Kacaniova, M. Elhourri, and M. Atanassova. Banana Peels: A Waste Treasure for Human Being. . *Evidence Based Complementary and Alternative Medicine*, **2022**:7616452, (2022).
DOI: https://doi.org/10.1155/2022/7616452.

[42] S. Maksoud, R.M. Abdel-Massih, H.N. Rajha, N. Louka, F. Chemat, F.J. Barba, and E. Debs. Citrus aurantium L. Active Constituents, Biological Effects and Extraction Methods. An Updated Review. . *Molecules*, **26**:5832, (2021).
DOI: https://doi.org/10.3390/molecules26195832.

[43] V. Revathi, S. Bora, N. Afzia, and T. Ghosh. Orange peel composition, biopolymer extraction, and applications in paper and packaging sector: A review. . *Sustainable Chemistry and Pharmacy*, **43**:101908, (2025).
DOI: https://doi.org/10.1016/j.scp.2025.101908.

[44] A. Fathia. Etude et valorisation des feuilles d'olivier Olea europeae dans l'industrie agroalimentaire. Thèse de doctorat en génie biologique. Université de Carthage (Tunisie). .

[45] K. Ghedira and P. Goetz. *Symphytum officinale* L. (Boraginaceae). . *Phytothérapie*, **10**:382–386, (2012).
DOI: https://doi.org/10.1007/s10298-012-0745-7.

[46] B. Salehi, F. Sharopov, T. Boyunegmez Tumer, A. Ozleyen, C. Rodriguez-Perez, S.M. Ezzat, E. Azzini, T. Hosseinabadi, M. Butnariu, I. Sarac, C. Bostan, K. Acharya, S. Sen, K. Nur Kasapoglu, C. Daskaya-Dikmen, B. Özcelik, N. Baghalpour, J. Sharifi-Rad, P. Valere Tsouh Fokou, W.C. Cho, and N. Martins. Symphytum Species: A Comprehensive Review on Chemical Composition, Food Applications and Phytopharmacology. *Molecules*, **24**:2272, (2019).
DOI: https://doi.org/10.3390/molecules24122272.

[47] C. Liewhiran and S. Phanichphant. Influence of Thickness on Ethanol Sensing Characteristics of Doctor-bladed Thick Film from Flame-made ZnO Nanoparticles. ". *Sensors*, **7**:185–201, (2007).
DOI: https://doi.org/10.3390/s7020185.

[48] Y.H. Hu, Y.C. Chen, H.J. Xu, H. Gao, W.H. Jiang, F. Hu, and Y.X. Wang. Texture ZnO Thin-Films and their Application as Front Electrode in Solar Cells. *Engineering*, **2**:973–978, (2010).
DOI: https://doi.org/10.4236/eng.2010.212124.